



Contents lists available at ScienceDirect

Journal of Nuclear Materials

journal homepage: www.elsevier.com/locate/jnucmat

Creep behavior of ODS materials: A study of dislocations/precipitates interactions

J. Malaplate^{a,*}, F. Momprou^b, J.-L. Béchade^a, T. Van Den Berghe^a, M. Ratti^a^a Département des Matériaux pour le Nucléaire, CEA Saclay, 91191 Gif-sur-Yvette, France^b Centre d'Elaboration des Matériaux et d'Etudes Structurales – CNRS, BP 94347, 31055 Toulouse Cedex 4, France

ARTICLE INFO

Article history:

Available online 12 January 2011

ABSTRACT

Creep experiments performed at 650 °C and 250 MPa on MA957 and CEA-developed 18%Cr ferritic Oxide Dispersion Strengthened (ODS) steels emphasize the particular creep behavior of ODS alloys. To understand the influence of oxide particles, we focused on the dislocation microstructure and their interaction mechanisms with precipitates. Microstructural characterization were performed using Transmission Electron Microscopy (TEM) on both un-deformed alloys and on 650 °C–250 MPa creep tested MA957 samples. No noticeable differences were observed, and dislocations seem to be anchored by precipitate particles. The dynamic behavior was studied by in situ TEM straining experiments at room temperature on MA957. Observation of dislocation motions indicates that interactions with particles, including pinning, control the flow stress at least at room temperature. At 650 °C, other mechanism is probably predominant.

© 2011 Elsevier B.V. All rights reserved.

1. Introduction

Advantages of the ferritic/martensitic steels (high thermal conductivity, low thermal expansion coefficient, and in particular good resistance to void swelling) make them candidate materials for fusion power plant first wall and blanket structures, and for fuel cladding and structural applications in Generation IV fission reactors. However, the upper operating temperature would be limited to 550–600 °C to avoid large deformation, especially during creep. Oxide dispersion (usually Y₂O₃) is a way to improve their mechanical properties [1–3], without losing ferritic/martensitic advantages, especially their resistance to void swelling [4–6].

Many studies have been completed on Oxide Dispersion Strengthened (ODS) alloys, however, the strengthening mechanisms associated with the deformation mechanisms, i.e. the interaction between precipitates and dislocations has not yet been clearly identified.

In this work, we focused on the creep behavior of two ODS alloys and then on the microstructure of commercial ODS alloy MA957 before and after creep deformation using Transmission Electron Microscopy (TEM). In situ TEM straining experiments

were also performed at room temperature to analyse the deformation mechanism leading to the oxide dispersion strengthening.

2. Experimental procedure

The commercial ODS ferritic alloy MA957 from INCO and a 18%Cr ferritic alloy developed by the CEA (referred as CEA 18%Cr-ODS) were used for creep tests. Their nominal compositions in wt.% are Fe–14Cr–0.3Mo–1.0Ti–0.25Y₂O₃ and Fe–18Cr–1W–0.3Ti–0.5Y₂O₃, respectively. The CEA 18%Cr alloy was produced by mechanical alloying, hot extrusion at 1100 °C, hot rolling 20% at 700 °C and finally annealing at 1050 °C. Cylindrical samples were cut from the MA957 rod (with longitudinal direction (LD) parallel to the extrusion direction) and coupon samples were cut from the 18%Cr rectangular shape rod (with longitudinal direction parallel to the extrusion direction). Creep tests were carried out at 650 °C and 250 MPa for both alloys.

TEM samples were prepared from MA957 before and after creep deformation. Specimens were mechanically thinned down to about 100 μm (70 μm for in situ straining). Punched 3 mm diameter TEM discs and 3 by 1 mm TEM in situ rectangles were electropolished at –10 °C in a 10% perchloric acid, 90% ethanol solution.

TEM observations were performed on a 2010FEG JEOL and a 430 FEI operating at 200 kV and 300 kV respectively. In situ TEM straining experiments were carried out on a 2010 JEOL equipped with a 25 frames per second camera. A Zeiss analyzer was used to study the precipitation size and distribution.

* Corresponding author. Address: DEN-DANS/DMN/SRMA/LA2M, Bat. 453, Pce 15C CEA, Saclay, 91191 Gif-sur-Yvette, France. Tel.: +33 (0)1 69 08 93 12; fax: +33 (0)1 69 08 71 30.

E-mail addresses: joel.malaplate@cea.fr (J. Malaplate), momprou@cemes.fr (F. Momprou), jean-luc.bechade@cea.fr (J.-L. Béchade), thierry.vandenbergh@cea.fr (T. Van Den Berghe), mathieu.ratti@cea.fr (M. Ratti).

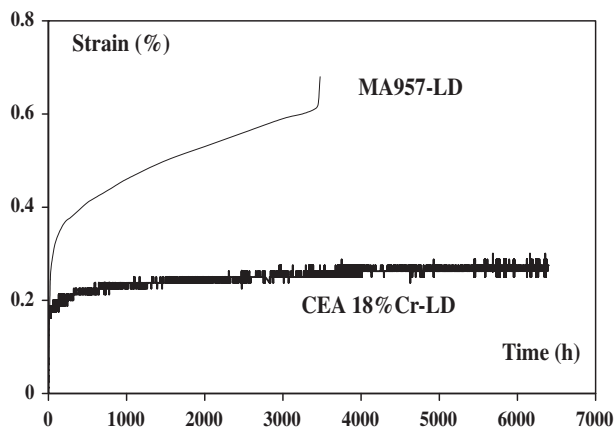


Fig. 1. Creep curves of MA957 and 18%Cr-ODS at 650 °C and 250 MPa.

3. Results and discussion

3.1. Creep curves

Fig. 1 shows creep curves obtained at 650 °C under a tensile stress of 250 MPa. CEA 18%Cr-ODS LD shows a higher creep resistance than MA957 LD, since MA957 LD failed after about 3500 h. The test on the CEA 18%Cr-ODS LD sample is still running.

From this figure, two important points must be emphasized: first, it can be noticed that the deformation remains low for the two alloys (rupture elongation is reached after only a few percents of strain) and second, MA957 LD, shows little or no tertiary creep, i.e. acceleration creep is almost absent. Although failure has not been reached for the CEA 18%Cr-ODS sample, the same trend can be observed for this alloy at higher stresses. This behavior is common to ODS alloys, as for instance in DY, DT [7], 14YWT [8], dual phase 9Cr-ODS [9], 8Cr J1 and J2 [10]. The particular shape of the ODS creep curve can probably be associated to the fine oxide dis-

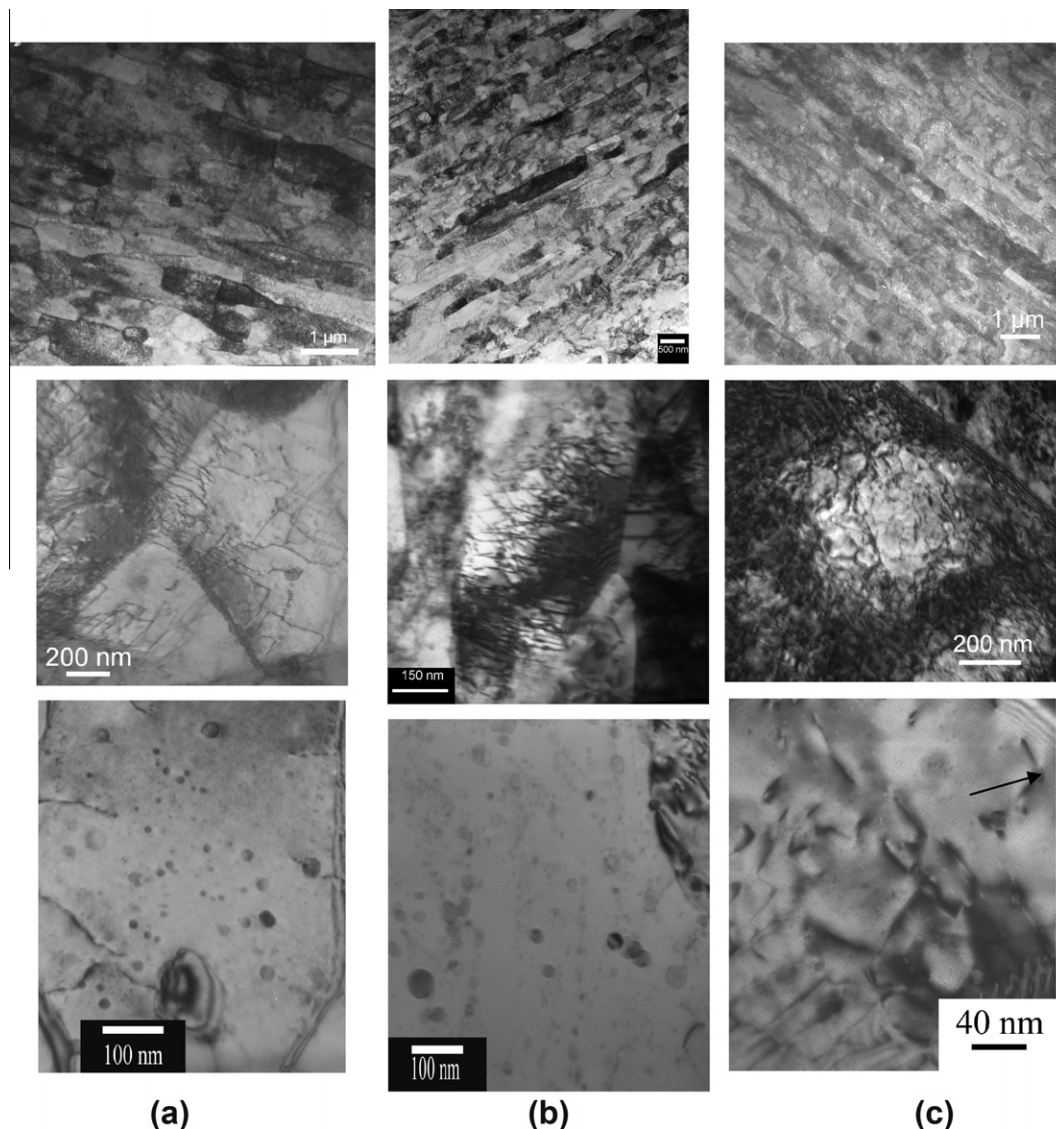


Fig. 2. Microstructure (a) of MA957 and (b) CEA 18%Cr-ODS before deformation and (c) of MA957 after creep at 650 °C 250 MPa (dislocation pinned on precipitate is indicated by arrow).

person. These ODS alloys also exhibit a high stress exponent [7,9,11], around 20 for MA957 LD.

3.2. Deformation mechanisms

3.2.1. Microstructure before deformation

The microstructure of MA957 alloy is composed of micrometer grains elongated along the extrusion direction (Fig. 2a). The grain size distribution was measured and lead to a mean size of 1.5 μm by 600 nm. A high dislocations density was observed, with an estimated value of $3 \times 10^{14} \text{ m}^{-2}$. The dislocations appear to be pinned by obstacles (Fig. 2a). Precipitates of several tens of nanometers were observed in MA957 as in [2]. A fine dispersion of precipitates (<10 nm) was also present. The particle size and number density were estimated at 2 nm and 10^{23} m^{-3} , respectively. EDS analysis on this samples [11] confirmed the particles are Y-Ti-O. Similar particle size and composition have been determined by atom probe in another study of MA957 [12].

First microstructural observations of CEA 18%Cr-ODS indicate that the grains are also elongated in the extrusion direction (Fig. 2b); compared to MA957, a similar mean grain size (1.2 μm by 400 nm) and a slightly higher dislocation density (about 10^{15} m^{-2}) are observed. Dislocations are also pinned at obstacles. A nano-precipitate dispersion was also identified. Estimated particles size and density are comparable to MA957.

3.2.2. In situ deformation at room temperature

In situ TEM straining tests were performed on MA957 samples cut parallel or perpendicular to the extrusion direction. They show dislocations moving jerkily between two positions where they stay pinned. While pinned, the dislocations bow-out under stress. When the stress is high enough, the dislocations quickly move to the next pinning point. Similar observations were made in samples cut perpendicular or parallel to the extrusion direction, indicating that at room temperature plasticity is controlled by intragranular mechanisms. Intergranular mechanisms (grain boundary sliding, cavitation) may operate at higher temperatures. These mecha-

nisms have to be investigated in order to explain the creep properties.

Dislocation Burgers vectors were found to be $\frac{1}{2}(111)$. The dislocations, preferentially aligned along their screw direction, glide in the (110) planes. Their preferential alignment and their jerky motion indicate that the friction stress is high. Their screw part quickly increases due to the faster motion of their edge part (Fig. 3). Bowing-out and un-pinning of screw parts was also observed but less often. When observed, the motion of screw segments appears jerky over distances larger than the mean inter-particles spacing. This indicates that screw segments move at a stress larger than the stress required to overcome oxide precipitates. This shows that the Peierls stress controls the motion of the screw segments and is larger than the stress required to overcome oxide particles. Because dislocation glide in a Peierls potential is a thermally activated motion, a different behavior can be expected at higher temperature.

The edge dislocation segments are probably stopped by nano-precipitates. Due to the small size of the precipitates, it is difficult to surely observe the precipitates on the dislocations. However the distance between two pinning points, ranging from 70 to 90 nm, is in good agreement with the estimated distance between two precipitates from the nano-precipitation analyses on the un-deformed samples (Section 3.2.1). The same order of magnitude can be found for other ODS alloys [9,13].

Dislocations piled up at grain boundary and dislocation source (single arm type) have also been observed.

TEM observations seem to indicate that the motion of the dislocations is controlled by the passing of the nano-precipitates. The back stress can be estimated in a first approximation, by measuring the curvature radius R of the dislocation line before the precipitate is overcome [14]:

$$\tau_b = \frac{\mu b}{4\pi(1-\nu)R} \ln \left\{ \frac{R}{r_0} \right\} \quad (1)$$

with $\mu = 90 \text{ GPa}$, $b = 0.248 \text{ nm}$, $r_0 = b$, $R \approx 40 \text{ nm}$, $\nu = 0.3$, this yields $\tau_b \approx 376 \text{ MPa}$.

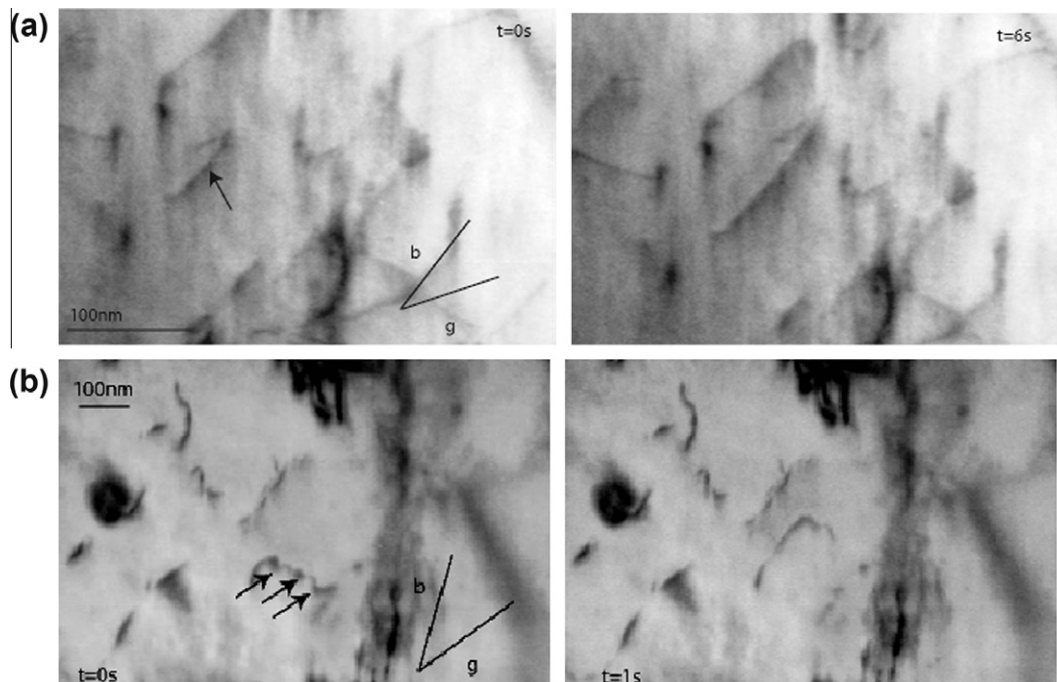


Fig. 3. Moving dislocations at room temperature (a) increasing of the screw part by edge part motion (b) un-pinning and re-pinning of an edge part (oxide pinning points are indicated by arrows).

In [13], the authors also performed in situ TEM straining experiments at room temperature on an ODS alloy, called MA956. The back stress value obtained in that case was lower. It is consistent with the higher strengthening in MA957 as usually observed in tensile tests [1]. These authors also concluded that the Orowan mechanism is operative at these low temperatures. Even if an evaluation of the Orowan stress, $\tau_{oe} \approx 130$ MPa [15] is close to the measured back stress, clear evidence of Orowan loops around precipitates are still missing. Further experiments should focus on this point.

Based on the results of dislocation density before deformation, the Taylor hardening ($\sigma = M\alpha\mu b\rho^{1/2}$) can be estimated around 450 MPa. We can then reasonably assume that precipitates/dislocations, dislocations/dislocations interactions and the friction stress are the three main contributions to the flow stress at room temperature.

3.2.3. Deformation at high temperature

TEM observations of creep tested samples did not reveal large microstructural differences with the un-deformed samples (Fig. 2c). A high dislocation density was still present (about $4 \times 10^{14} \text{ m}^{-2}$), and the dislocations were also pinned on precipitates. Nevertheless, the interaction mechanisms proposed at room temperature are probably less efficient at these higher temperatures and then may not control the flow stress anymore. Indeed, the noticeable decrease of the flow stress observed in these materials [1] above 400 °C could suggest that particles can be more easily overcome by thermal activation. The theory of Rösler and Arzt [16], assuming that after overcoming the particle by climb the dislocations become pinned at their departure side, might be considered. This theory is based on an “attractive” interaction resulting from a dislocation located on the “exit” of the clusters. Although it is difficult to observe dislocation behavior to the precipitate scale, this mechanism could be effective in our samples. As already suggested, due to precipitates loss of efficiency at high temperature, alternative mechanisms could become more important. For instance, studies on MA957 [2] have shown that at temperatures above 600 °C, the grain size has an influence on the creep rate, suggesting also that mechanisms involving diffusion towards grain boundaries can be efficient. These mechanisms could play a significant role in our fine grain microstructure. In particular, the similarity of the microstructure of MA957 and CEA 18%Cr-ODS (Section 3.2.1) suggests that the intragranular plasticity is equivalent for these two alloys. Therefore, the differences in creep behavior should not come from particles/dislocations interactions, but from other processes.

It would be interesting to perform in situ straining experiments at room temperature on the CEA 18%Cr-ODS to confirm that the particles/dislocations interactions are similar to MA957. Then it

would also be interesting to perform high temperature in situ straining experiments on these alloys to give a dynamic insight into the deformation mechanisms. Indeed, although the microstructure before deformation of the two ODS alloys seems to be quite equivalent, the CEA 18%Cr-ODS alloy exhibits better creep behavior. Such type of experiments would be helpful to investigate the origin of this discrepancy.

4. Summary

The creep behavior of ODS alloys was addressed, focusing on the dislocations/nano-precipitate interaction mechanisms. MA957 and CEA 18%Cr-ODS alloys exhibit a “non-classical” creep behavior, with low creep strain and no tertiary creep regime. At room temperature, first results obtained by in situ TEM straining experiments show that nano-precipitates are strong obstacles to the dislocation glide. After creep at high temperature, TEM observations reveal that dislocations are still pinned, confirming that nano-precipitates still play a role on the creep behavior at higher temperature.

References

- [1] R.L. Klueh, J.P. Shingledecker, R.W. Swindeman, D.T. Hoelzer, *J. Nucl. Mater.* 341 (2005) 103–114.
- [2] A. Alamo, V. Lambard, X. Averty, M.H. Mathon, *J. Nucl. Mater.* 329–333 (2004) 333–337.
- [3] R. Lindau, A. Möslang, M. Rieth, M. Klimiankou, E. Materna-Morris, A. Alamo, A.-A.F. Tavassoli, C. Cayron, A.-M. Lancha, P. Fernandez, N. Baluc, R. Schäublin, E. Diegele, G. Filacchioni, J.W. Rensman, B.V.D. Schaaf, E. Lucon, W. Dietz, *Fus. Eng. Design* 75–79 (2005) 989–996.
- [4] M.B. Toloczko, D.S. Gelles, F.A. Garner, R.J. Kurtz, K. Abe, *J. Nucl. Mater.* 329–333 (2004) 352–355.
- [5] H. Kishimoto, K. Yutani, R. Kasada, O. Hashitomi, A. Kimura, *J. Nucl. Mater.* 367–370 (2007) 179–184.
- [6] R. Schäublin, A. Ramar, N. Baluc, V. de Castro, M.A. Monge, *J. Nucl. Mater.* 351 (2006) 247–260.
- [7] C. Zakine, Ph.D. Thesis, Ecole Centrale Paris, 1994.
- [8] T. Hayashi, P.M. Sarosi, J.H. Schneibel, M.J. Mills, *Acta Mater.* 56 (2008) 1407–1416.
- [9] H. Sakasegawa, S. Ukai, M. Tamura, S. Ohtsuka, H. Tanigawa, H. Ogiwara, A. Kohyama, M. Fujiwara, *J. Nucl. Mater.* 373 (2008) 82–89.
- [10] K. Shinozuka, M. Tamura, H. Esaka, K. Shiba, K. Nakamura, *J. Nucl. Mater.* 384 (2009) 1–5.
- [11] H. Sakasegawa, L. Chaffron, F. Legendre, M. Brocq, L. Boulanger, S. Poissonnet, Y. de Carlan, J.-L. Béchade, T. Cozzika, J. Malaplate, *J. Nucl. Mater.* 386 (2009) 511–514.
- [12] M.K. Miller, D.T. Hoelzer, E.A. Kenik, K.F. Russell, *J. Nucl. Mater.* 329–333 (2004) 338–341.
- [13] M. Bartsch, A. Wasilkowska, A. Czyrska-Filemonowicz, U. Messerschmidt, *Mater. Sci. Eng.* A272 (1999) 152–162.
- [14] J.P. Hirth, J. Lothe, *Theory of Dislocations*, second ed., A Wiley-Interscience Publication, 1982.
- [15] D.J. Bacon, U.F. Kocks, *R.O. Scattergood, Phil. Mag.* 28 (1973) 1241–1263.
- [16] J. Rösler, E. Arzt, *Acta Metall. Mater.* 38 (1990) 671–683.